FROM LABORATORY SNR TO OPERATIONAL IMAGE QUALITY: EVALUATING SCENE-DERIVED APPARENT SNR IN AIRBORNE HYPERSPECTRAL IMAGERY

Simon A. Trim[*]*, Andreas Hueni*

Remote Sensing Laboratories, Department of Geography,
University of Zurich,
Zurich, Switzerland

Daniel Schläpfer

ReSe Applications LLC,
Langeggweg 3,
CH-9500 Wil, Switzerland

ABSTRACT

Laboratory signal-to-noise ratio (SNR) characterizes sensor performance under controlled conditions, whereas operational hyperspectral imagery additionally reflects atmospheric, illumination, and scene effects. We evaluate a scene-derived apparent SNR estimator based on adjacent-band spectral differencing and local residual statistics using HySpex Mjolnir and AVIRIS-4 imagery. Spatial apparent SNR maps are summarized by robust band-wise statistics and compared with independent laboratory or calibration-based SNR characterization. Apparent SNR showed strong spectral correspondence with calibration-based models for Mjolnir V1240 (Pearson $r = 0.88$) and S620 ($r = 0.98$), despite systematically lower magnitudes. AVIRIS-4 showed moderate correspondence with integrating-sphere laboratory measurements ($r = 0.44$), with pronounced apparent SNR reductions around atmospheric water vapor absorption regions. These results indicate that the estimator captures wavelength-dependent instrument behavior while remaining sensitive to conditions affecting acquired imagery. Apparent SNR is therefore interpreted as an operational complement to, rather than a replacement for, laboratory SNR characterization.

***Index Terms*—** Hyperspectral imaging, signal-to-noise ratio, data quality assessment, imaging spectroscopy, spectral differencing

1. INTRODUCTION

Signal-to-noise ratio (SNR) is a fundamental measure of hyperspectral imaging (HSI) quality, affecting the reliability of subsequent spectral analysis and retrieval. Instrument SNR is commonly characterized under controlled laboratory conditions, where illumination, signal level, and acquisition parameters can be prescribed [1]. Such characterization is essential for quantifying sensor performance, but the signal quality manifested in operational imagery additionally depends on acquisition conditions, atmospheric propagation, illumination, and the spectral and spatial properties of the observed scene. Hyperspectral noise itself may contain multiple spectrally and spatially varying contributions [2].

Image-based SNR estimation provides a complementary means of assessing data quality directly from acquired imagery. Established approaches estimate noise from spatial statistics within sufficiently homogeneous image regions [3]. For hyperspectral imagery, however, the strong correlation between adjacent spectral bands also provides information that can be exploited for noise estimation. Spectral differencing can suppress locally smooth spectral signal while retaining high-frequency residual variability, allowing signal quality to be characterized without requiring dedicated homogeneous calibration targets. The resulting residual is not necessarily attributable to instrumental noise alone: genuine spectral curvature, atmospheric structure, calibration residuals, and local scene variability may also contribute.

Integrated into INTACOR®, an automatic geometric and atmospheric correction and processing pipeline, the Data Quality Assessment (DQA) workflow applies this spectral differencing principle to derive spatially resolved *apparent SNR* directly from calibrated HSI radiance [4]. Local residual statistics provide an apparent SNR map for each spectral band, from which robust band-wise statistics can be derived. The term *apparent SNR* distinguishes this image-derived quantity from laboratory instrument SNR because it intentionally characterizes the quality manifested in a particular acquired scene.

This study evaluates the relationship between scene-derived apparent SNR and independent laboratory (calibration-based) SNR characterization. The method is applied to operational imagery from two imaging systems: the VNIR and SWIR sensors of the HySpex Mjolnir VS-620 [5] and the VNIR–SWIR AVIRIS-4 imaging spectrometer [6]. Band-wise apparent SNR behavior is compared with calibration-based SNR models for Mjolnir and integrating sphere laboratory measurements for AVIRIS-4. The objective is not to reproduce laboratory SNR from a single image, but to determine to what extent the scene-derived metric retains wavelength-dependent sensor behavior and where operational acquisition effects cause the two measures to diverge.

[*] Also with ReSe Applications LLC.

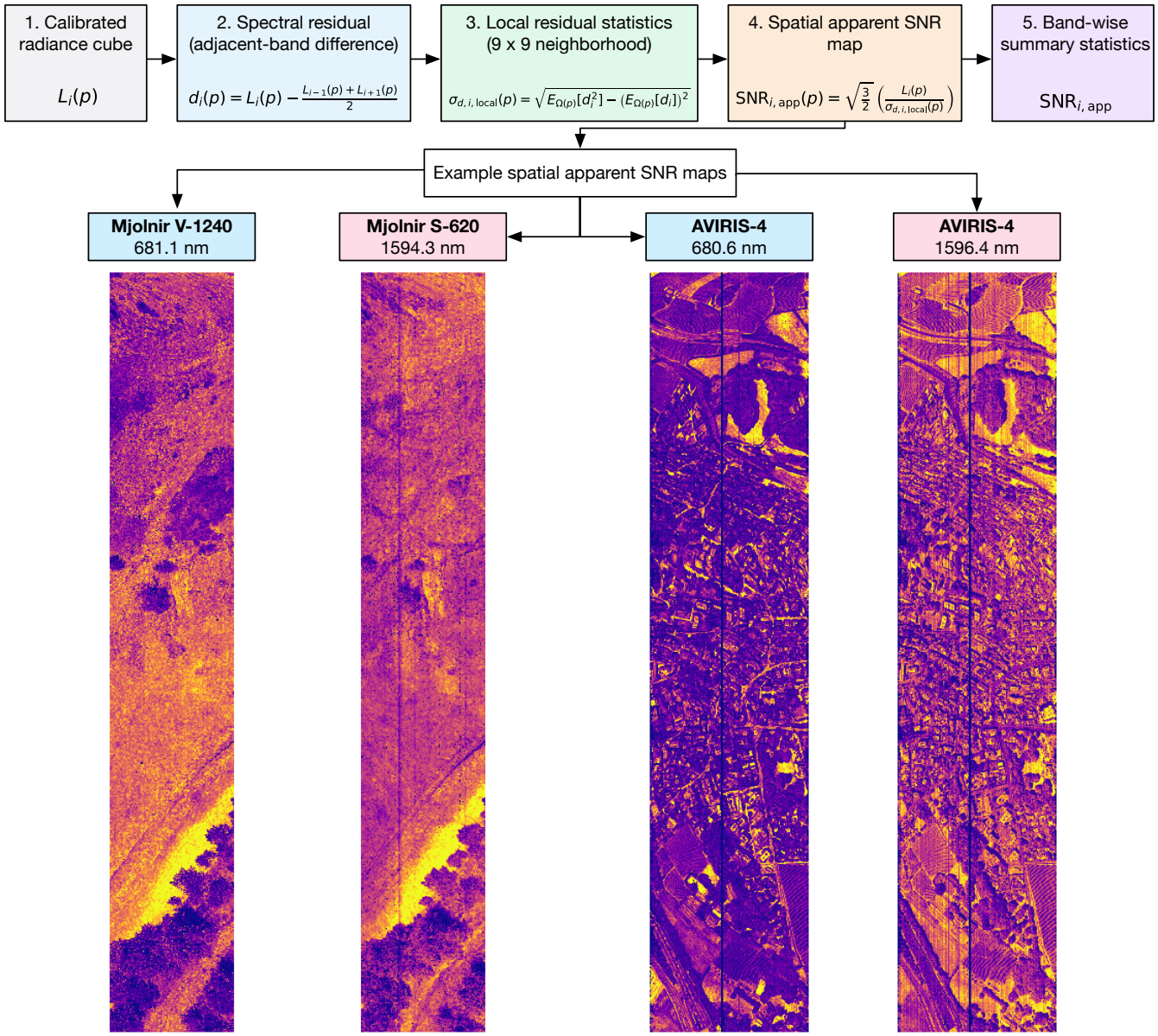


Fig. 1. Apparent SNR estimation workflow and representative spatial outputs at spectrally matched VNIR and SWIR wavelengths. Spatial residual statistics are calculated within a 9×9 pixel neighborhood. Maps are independently scaled to the 2nd–98th percentile of valid apparent SNR values for visualization. The Mjolnir data was acquired in 2024 at the legacy Memi Mine (Republic of Cyprus) during a field campaign by m4mining [7]. The AVIRIS-4 data was acquired in July 2026 over Colombier (Switzerland) in the context of a test flight by the ARES Observatory [8].

2. SCENE-DERIVED APPARENT SNR ESTIMATOR

The apparent SNR estimator exploits the high band-to-band correlation of hyperspectral radiance through adjacent-band spectral differencing (Fig. 1). For each spatial pixel p and spectral band i, the residual is

$$d_i(p) = L_i(p) - \frac{L_{i-1}(p) + L_{i+1}(p)}{2}, \qquad (1)$$

where $L_i(p)$ is the measured radiance. Assuming a locally smooth spectrum and independent, zero-mean noise of approximately equal variance σ^2 in the three adjacent bands, $\mathrm{Var}(d_i) = 3\sigma^2/2$ and the single-band noise standard deviation is estimated as $\hat{\sigma}_i = \sigma_{d,i}/\sqrt{3/2}$. Spectral differencing suppresses locally smooth signal components, but genuine spectral structure may remain in the residual; hence the resulting quantity is termed *apparent SNR*.

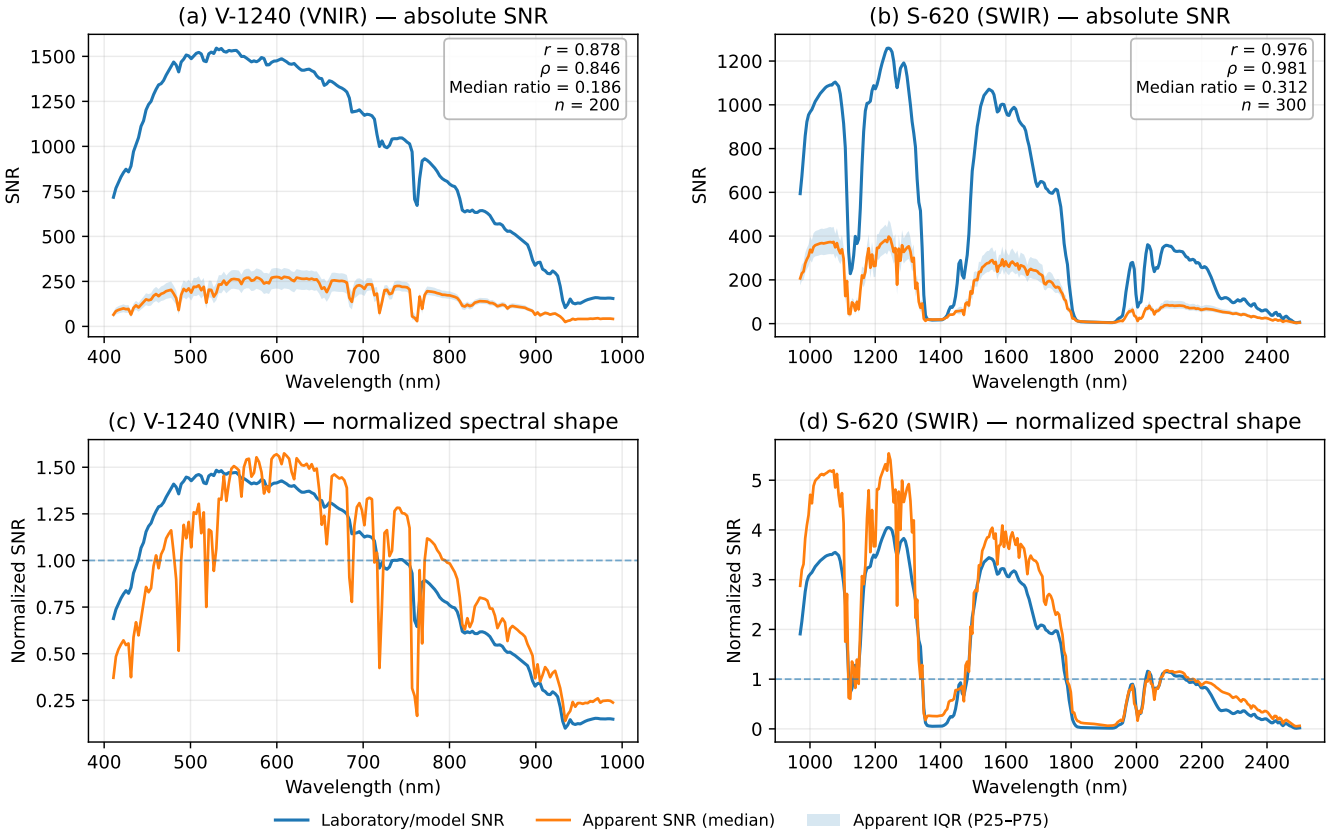


Fig. 2. Scene-derived apparent SNR and calibration-based SNR models for Mjolnir V-1240 (left) and S-620 (right), shown in absolute (top) and median-normalized form (bottom). Shading denotes the 25th–75th percentile of spatial apparent SNR. Pearson r, Spearman ρ, and the median apparent-to-model SNR ratio are reported for each sensor (with n the number of bands).

For spatially resolved estimation, the residual variance is calculated within a 9×9 pixel neighborhood $\Omega(p)$ using valid pixels:

$$\sigma^2_{d,i,\mathrm{local}}(p) = E_{\Omega(p)}[d_i^2] - \left(E_{\Omega(p)}[d_i]\right)^2 . \tag{2}$$

The spatial apparent SNR is then

$$\mathrm{SNR}_i(p) = \sqrt{\frac{3}{2}} \left(\frac{L_i(p)}{\sigma_{d,i,\mathrm{local}}(p)} \right) . \tag{3}$$

Low-signal pixels are excluded from the DQA statistics. Band-wise apparent SNR is represented by the median of the valid spatial estimates,

$$\mathrm{SNR}_{i,\mathrm{band}} = \underset{p \in V_i}{\mathrm{median}} \left[\mathrm{SNR}_i(p) \right] , \tag{4}$$

with the 25th and 75th percentiles characterizing within-scene spatial variability. Thus, the same local estimator provides both spatial apparent SNR maps (Fig. 1) and their robust wavelength-dependent summaries (Figs. 2 and 3).

3. RESULTS AND DISCUSSION

3.1. Mjolnir comparison

Scene-derived apparent SNR shows strong spectral correspondence with the calibration-based Mjolnir models (Fig. 2): $r = 0.878$ and $\rho = 0.846$ for V-1240 ($n = 200$), and $r = 0.976$ and $\rho = 0.981$ for S-620 ($n = 300$). The normalized curves demonstrate that wavelength-dependent behavior is retained independently of absolute magnitude.

Apparent SNR was systematically lower, with median apparent-to-model ratios of 0.186 (V-1240) and 0.312 (S-620). This difference is not an estimation error: the calibration models characterize sensor performance under specified conditions, whereas the scene-derived metric additionally responds to signal level and spectral-spatial scene properties.

3.2. AVIRIS-4 comparison

AVIRIS-4 shows weaker correspondence with integrating sphere laboratory SNR (Fig. 3), with $r = 0.441$, $\rho = 0.432$, and a median apparent-to-laboratory ratio of 0.158 across

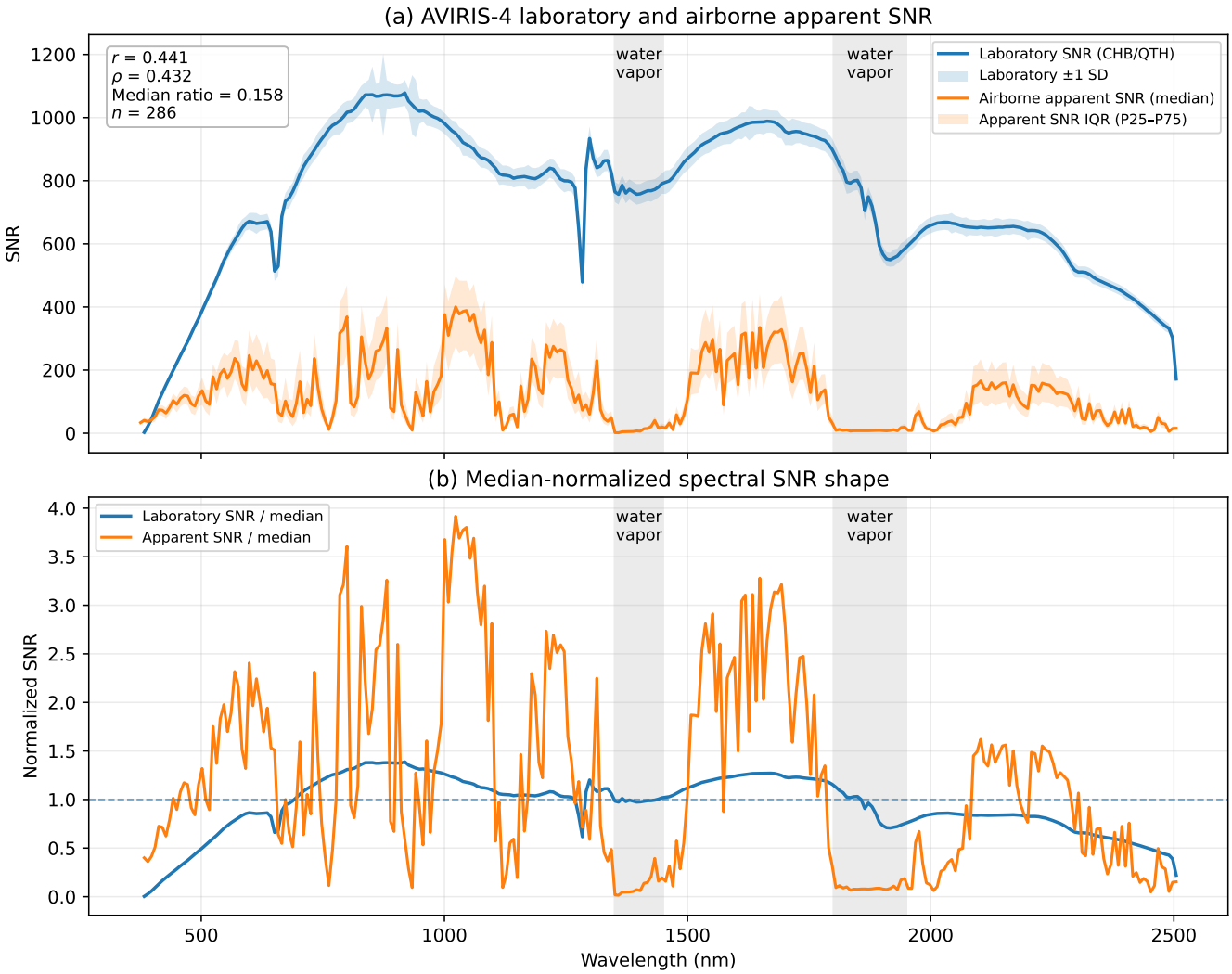


Fig. 3. Scene-derived AVIRIS-4 apparent SNR and integrating sphere laboratory SNR measured at the DLR Calibration Home Base [9], shown in absolute (top) and median-normalized form (bottom). Shading denotes spatial apparent SNR variability and across-track laboratory variability; vertical bands mark major atmospheric water vapor absorption regions.

286 matched bands. As expected, the largest discrepancies occur around the atmospheric water vapor absorption regions near 1.4 and 1.9 μm, where airborne apparent SNR decreases sharply while laboratory SNR remains comparatively high. Atmospheric and surface spectral structure, calibration residuals, and local scene variability may remain after adjacent-band differencing; the residual therefore cannot generally be interpreted as detector noise alone.

Acquisition geometry may contribute to the stronger atmospheric imprint: the Mjolnir data were acquired from a UAS at $\leq$ 100 m above ground, compared with a mean altitude of 757 m for the AVIRIS-4 acquisition. However, the instruments, scenes, illumination, spatial resolution, and reference SNR methodologies also differ, precluding attribution to atmospheric path length alone.

Laboratory SNR itself is signal- and wavelength-dependent. Figure 4 shows AVIRIS-4 focal-plane SNR varying nonlinearly with dark current-corrected digital numbers, with additional wavelength-dependent structure. This further illustrates that laboratory and scene-derived SNR describe related but distinct aspects of hyperspectral data quality.

3.3. Implications and limitations

Across both systems, apparent SNR reproduces wavelength-dependent instrument behavior to varying degrees while remaining sensitive to operational image conditions. This sensitivity is useful for data quality assessment because atmospheric absorption, low signal, and local scene variability may reduce the utility of acquired data even when the detector

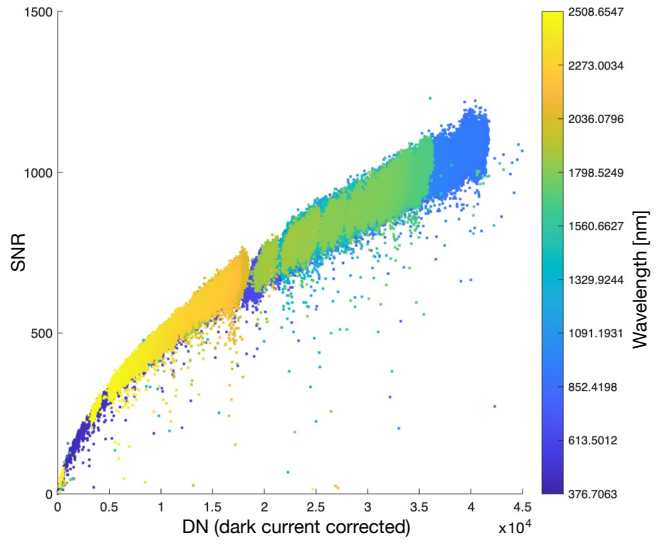


Fig. 4. Laboratory SNR of AVIRIS-4 focal-plane-array pixels as a function of dark current-corrected digital numbers (DN) for QTH lamp combination 8 (points colored by wavelength).

performs nominally. Apparent SNR should therefore be interpreted as an operational complement to, rather than a replacement for, laboratory characterization.

The estimator assumes locally smooth spectra and independent, approximately equal-variance noise in adjacent bands. Genuine spectral curvature, inter-band noise correlation, and spatial heterogeneity within the 9×9 neighborhood may therefore influence the estimates. Furthermore, the two imaging systems were evaluated using different scenes, platforms, and reference SNR methodologies; the present comparison consequently demonstrates cross-instrument applicability rather than a controlled sensor intercomparison.

4. CONCLUSION AND OUTLOOK

Comparison across Mjolnir and AVIRIS-4 data demonstrates that scene-derived apparent SNR preserves meaningful wavelength-dependent information about HSI quality without being equivalent to laboratory SNR. The differing correspondence observed between the two systems further shows that the metric responds to the conditions under which the imagery is acquired. Its value therefore lies in assessing the spectral and spatial quality actually manifested in operational radiance data.

Future work will evaluate additional sensors and acquisition conditions and investigate the influence of atmospheric and scene contributions, local-window size, spectral curvature, and correlated inter-band noise. Signal-dependent models may ultimately provide a means of linking controlled laboratory characterization with SNR expected under operational radiance conditions.

5. REFERENCES

[1] John Woodward, Steven Brown, Allan Smith, and Keith Lykke, "Hyperspectral Imager Characterization and Calibration," in *2009 IEEE Internation Geoscience and Remote Sensing Symposium, Cape Town, -1*, 2009, p. https://doi.org/10.1109/IGARSS.2009.5418005.

[2] Behnood Rasti, Paul Scheunders, Pedram Ghamisi, Giorgio Licciardi, and Jocelyn Chanussot, "Noise reduction in hyperspectral imagery: Overview and application," *Remote Sensing*, vol. 10, no. 3, pp. https://doi.org/10.3390/rs10030482, 2018.

[3] Bo-Cai Gao, "An operational method for estimating signal to noise ratios from data acquired with imaging spectrometers," *Remote Sensing of Environment*, vol. 43, no. 1, pp. 23 – 33. https://doi.org/10.1016/0034–4257(93)90061–2, 1993.

[4] Simon A. Trim and Daniel Schläpfer, "Automated Radiance-Level Data Quality Assessment for Hyperspectral Imaging," in *2025 15th Workshop on Hyperspectral Imaging and Signal Processing: Evolution in Remote Sensing (WHISPERS)*, 2025, pp. 1–5.

[5] Norsk Elektro Optikk AS, "HySpex Mjolnir VS-620," https://www.hyspex.com/hyspex-products/hyspex-mjolnir/mjolnir-vs-620 (accessed September 23rd, 2026), 2026.

[6] Andreas Hueni, Sven Geier, Marius Vögtli, Jesse LaHaye, Josquin Rosset, Dominic Berger, Luc J. Sierro, Laurent V. Jospin, David R. Thompson, Daniel Schläpfer, Robert O. Green, Teddy Loeliger, Jan Skaloud, and Michael E. Schaepman, "The AVIRIS-4 Airborne Imaging Spectrometer," *IEEE Geoscience and Remote Sensing Letters*, vol. 22, pp. 1–5, 2025.

[7] Ekaterina Savinova, Friederike Koerting, Daniel Schläpfer, Nicole Koellner, Ioulia Georgiadou Gavrilovic, Irene C. Christoforou, and Justus Constantin Hildebrand, "Multiscale Remote Sensing and Ground Truth Dataset for Mine Waste Characterisation at Memi Mine, Republic of Cyprus (m4mining project) ," Sept. 2026.

[8] ARES Observatory, "Airborne Research of the Earth System," https://ares-observatory.ch/ (accessed September 23rd, 2026), 2026.

[9] Andreas Baumgartner, Gabriel Arden Scheib, and Konstantin Torgasin, "DLR's Calibration Home Base for Imaging Spectrometers (CHB)," in *FRM4drones-AQUATIC Workshop 2: Uncertainty, FRM, and Traceability*, 2025.